

# Non-Destructive Sensing for Determining Sunagoke Moss Water Content Bio-inspired Approaches

Y. Hendrawan<sup>1</sup>, H. Murase<sup>1</sup>

<sup>1</sup>Bio-instrumentation, Control and Systems (BICS) Engineering Laboratory, Graduate School of Life and Environmental Sciences, Osaka Prefecture University  
1-1 Gakuen-cho, Sakai, Osaka 599-8531, Japan  
E-mail: yusuf@bics.osakafu-u.ac.jp

## ABSTRACT

One of the primary determinants of Sunagoke moss *Rachomitrium japonicum* growth is water availability. There is need to develop non-destructive sensing of Sunagoke moss water content to realize automation and precision irrigation in a closed bio-production system. Machine vision can be utilized as non-destructive sensing to recognize changes in some kind of features that describe the water conditions from the appearance of wilting Sunagoke moss. The goal of this study is to propose and investigate Bio-inspired algorithms *i.e.* Neural-Genetic Algorithms (neural-GA) and Neural-Ant Colony Optimization (neural-ACO) to find the most significant set of image features suitable for predicting cultured Sunagoke moss water content in a closed bio-production system. Features extracted consisted of 13 colour features, 90 textural features (grey, RGB, HSV and HSL colour co-occurrence matrix textural features) and three morphological features. Each colour space consisted of ten textural features algorithms: entropy, energy, contrast, homogeneity, sum mean, variance, correlation, maximum probability, inverse difference moment and cluster tendency. The specificity of this problem was that we were not looking for single image feature but several associations of image features that may be involved in determining water content of Sunagoke moss. The results show that neural-ACO has lower average validation set Mean Square Error (MSE) than neural-GA, but there is no significant difference between their prediction performances. Neural-ACO has better performance for selecting relevant features than neural-GA and there is significant statistical difference between them. Methods using feature selection technique has better result than methods without feature selection technique. Finally, ten relevant image features for predicting water content of Sunagoke moss were obtained from neural-ACO.

**Keywords:** Ant Colony Optimization, Features extraction, Feature selection, Genetic Algorithms, Machine vision, Sunagoke moss, Water content sensing.

## 1. INTRODUCTION

Sunagoke moss *Rachomitrium japonicum* is a good potential material for living roof and wall greening for urban heat island mitigation. Among all kinds of moss, Sunagoke moss is the most suitable for the greening of building surfaces (Ondimu and Murase, 2006). This moss can grow on inorganic materials such as concrete, because it does not need any soil and fertilizer for growing, nor does it add too much extra load to the building roof structure. Moreover, it is almost maintenance-free. Sunagoke moss is incapable of photosynthesis when the water content

is low. Higher water contents may actually decrease the rate of photosynthesis by increasing resistance to diffusion of CO<sub>2</sub> (Oechel and Collins, 1976). To establish water contents that are appropriate for its optimum rates of net fixation, the water states that trigger its deficit and excess water stresses need to be determined. Water affects evapotranspiration and canopy photosynthesis. Evaporation of plants is affected by many factors (Bacci *et al.*, 2008), both environmental (*e.g.*, air temperature, radiation and humidity) and plant related characteristics (*e.g.*, growth phase, leaf area, fresh weight, leaf water potential).

Sunagoke moss mats are being produced in tunnels as shown in figure 1. There are two important components during the production process: 1) illumination component as shown in figure 1(a) in which moss mats are given appropriate light condition to optimize photosynthesis process during cultivation; and 2) water condition as shown in figure 1(b) in which moss mats are sprayed proper amount of water. Irrigation is an essential component of moss production. Conventional irrigation as shown in figure 1(b) often applies a fixed water irrigation rate for the whole target and do not consider the variation in the spraying target area. Different parts of moss mat have different capacities to hold and transport water (Kellner, 2001). Water affects evapotranspiration and canopy photosynthesis, and hence net primary productivity. Therefore, there is need to develop non-destructive sensing of Sunagoke moss water content to realize automation and precision irrigation for Sunagoke moss production in tunnels.



Figure 1. Sunagoke moss production in tunnel: (a) illumination component; (b) water component.

There are many methods for sensing water condition in Sunagoke moss. The direct measurement of canopy parameters is considered to be relatively inefficient, destructive to the plants and can not always provide accurate results at the large scale production of Sunagoke moss in plant factory. Even a slight contact of foreign material with the plant tissue disturbs physiological activity of the plant (Murase *et al.*, 1997). It may be possible to recognize changes in some kind of features that describe the water conditions from the appearance of wilting Sunagoke moss by machine vision. Shape and textural features have been used for some time for pattern recognition in datasets such as remote sensed imagery, medical imagery, photographs, *etc.* (Newsam and Kammath, 2005). An analysis of the morphology of the plant features could be particularly useful to determine indicators that characterize the plant quality (Kurata and Yan, 1996; Recce *et al.*, 1996; Foucher *et al.*, 2004). Many studies have reported use combination of colour, morphology and textural features to detect stress in plant (Ahmad and Reid, 1996; Escos *et al.*, 2000; Leemans *et al.*, 2002). This study reports an attempt to evaluate the water content prediction ability of image features in Sunagoke moss. Non-linear relationships between image

features and water content can be identified by Back-Propagation Neural Network (BPNN). BPNN theory, generally accepted as a useful tool for the recognition of various patterns. Cybenko (1989) showed that a three-layer neural network with one hidden layer allowed any continuous function to be successfully identified.

Selecting features that are suitable for an application is one of the most important parts in solving the problem. Colour Features (CF), Morphological Features (MF) and Textural Features (TF) are all able to represent some information about image. The main problem is first to find efficient features for image representation, then to find effective measure that uses these representations, individually or as a combination. This study also reports an attempt to evaluate Bio-inspired algorithms (Genetic Algorithms (GA) and Ant Colony Optimization (ACO) as Feature Selection (FS) technique) to identify and remove as much irrelevant and redundant features as possible. FS techniques have become an apparent need in many bioinformatics applications (Handels *et al.*, 1999; Utku, 2000; Saeys *et al.*, 2007). Verma and Zhang (2007) observed how neural-GA (combination of Artificial Neural Network (ANN) and GA) for FS could classify microcalcification patterns in digital mammograms. They showed that neural-GA is able to find an appropriate feature-subset, which also produces a high classification rate. Hendrawan and Murase (2009) observed that wrapper technique (neural-GA) as FS method has better performance than filter techniques or statistical FS such as Chi-Squared, Mutual Information, Correlation-based Features Selection and Linear Regression for selecting relevant image features. In this study we will discuss on a novel approach of wrapper technique (neural-ACO) for selecting relevant image features and compare the performance with neural-GA.

The goal of this study is to propose and investigate Bio-inspired algorithms (Neural-GAs and Neural-ACO) to find the most significant sets of image features suitable for predicting water content of cultured Sunagoke moss using machine vision with the most minimum prediction error. Many researchers have analyzed feature selection techniques for prediction. As a result, the selection of the relevant subset has improved prediction accuracy. However, due to the small number of samples compared to the huge number of features dimension and irrelevant features, the most approaches face difficulties to select the relevant feature-subset. Therefore, the ultimate goal of this research is to propose intelligent approaches for selecting relevant subset of informative features from image data for predicting water content of Sunagoke moss.

## 2. MATERIALS AND METHODS

### 2.1 Materials and equipment

Study samples were made from living cultured Sunagoke moss mat *Rhacomitrium japonicum* (500 mm x 500 mm, M-300, VARORE Co., Japan) as shown in figure 2(a). The samples are made of living cultured Sunagoke moss growing in polyvinyl (PVC) netting and anchored in glass wool media. Ten samples of cultured Sunagoke moss (figure 2(b)), placed in a 110 mm x 80 mm x 25 mm glass vessel were used in this study. Distilled water was given to the samples in the amount of 4.0 gg<sup>-1</sup> (4.0 gram of water content per gram of initial dry weight). Water content was defined as the average amount of water available for each sample in each day of data acquisition in grams per gram of its initial dry weight. Water content was determined as:

$$\text{Water Content} = \frac{tw - dw}{dw} \quad (1)$$

where:  $tw$  is the total weight or wet weight (g) and  $dw$  is initial dry weight (g) of Sunagoke moss. Dry weight of moss was determined by drying it in the growth chamber (Biotron NK 350, Japan) with the optimum environment parameters (Hendrawan and Murase, 2008): air temperature = 15°C, RH = 80%, the CO<sub>2</sub> gas = 400 ppm, light intensity = 30 kflux, light duration = 12 h until the weight of moss was stabilized without any further decrement. The average initial dry weight of samples was 12.5 g. Each sample was soaked with 4.0 gg<sup>-1</sup> of water content and let to dry until it reached the initial dry weight (0 gg<sup>-1</sup>).

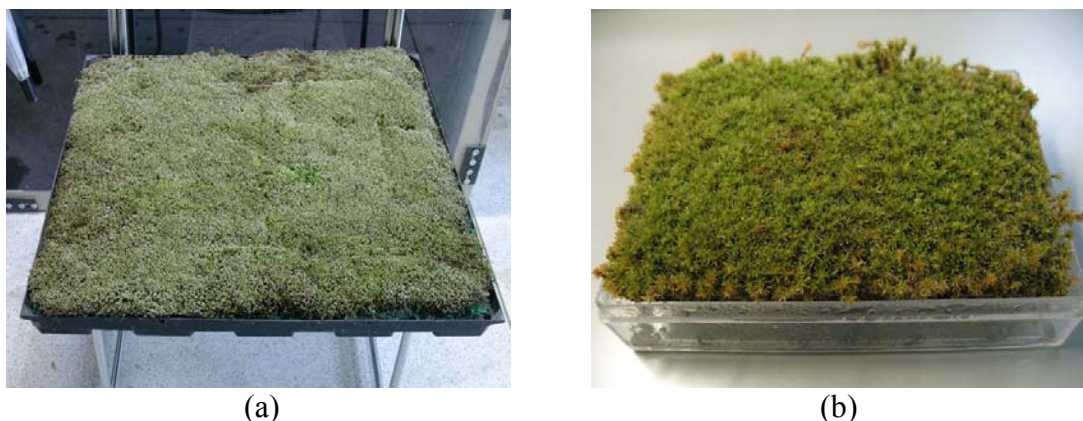


Figure 2. Cultured Sunagoke: (a) moss mat; (b) study sample.

## 2.2 Methods

The experimental design aiming at the prediction of Sunagoke moss water content is presented in figure 3. The first process is image acquisition, in which the moss images were captured using digital camera (Nikon Coolpix SQ, Japan) placed at 330 mm perpendicular to the sample surface as shown in figure 4. The image size was 1024 x 768 pixels with the spatial resolution of the images of 0.1 mm/pixel. Imaging was done under controlled and well distributed light conditions. Light was provided by two 22W lamps (EFD25N/22, National Corporation, Japan). Light intensity over the moss surface was uniform at 100  $\mu\text{mol m}^{-2} \text{s}^{-1}$  PPF (Photometer, Li6400, USA) during image acquisition. Light intensity was measured at five points on the moss surface area that were four points at the edge and one point at the middle part. In every image capturing process, the intensity of light was always measured to maintain the light condition to remain stable and uniform at 100  $\mu\text{mol m}^{-2} \text{s}^{-1}$  PPF. A total of 300 data images were acquired. All of 300 images obtained at image acquisition went through a transformation process to convert images from red-green-blue (RGB) colour space to hue-saturation-value (HSV), hue-saturation-lightness (HSL) and grey level colour spaces. Features extraction process extracted three different image features (CF, MF and TF). Then, the full feature sets, or their reduced versions obtained after proper FS in the FS process, were fed to a BPNN for predicting water content. Two alternative Bio-inspired approaches (GA and ACO) for conducting FS were studied. A comparison study was conducted to analyze the performance of each FS technique. All software included features extraction, BPNN, neural-GA and neural-ACO were built in Visual Basic 6.0 (self-built software).

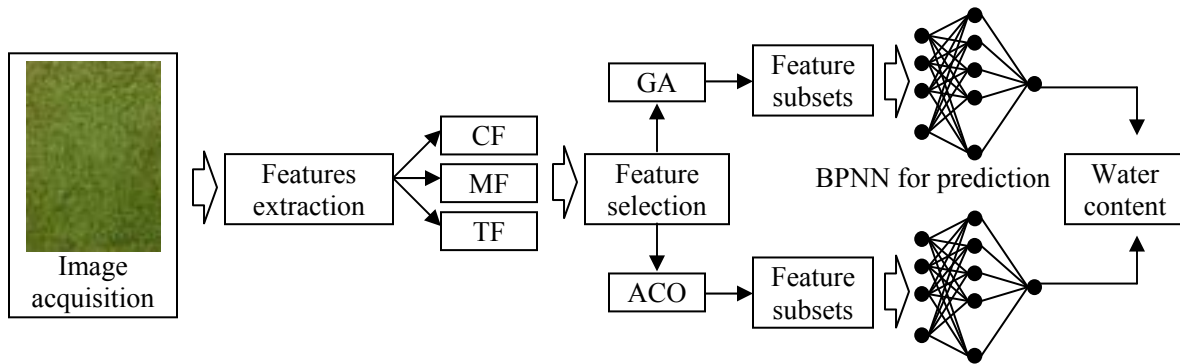


Figure 3. Non-destructive sensing for determining Sunagoke moss water content.

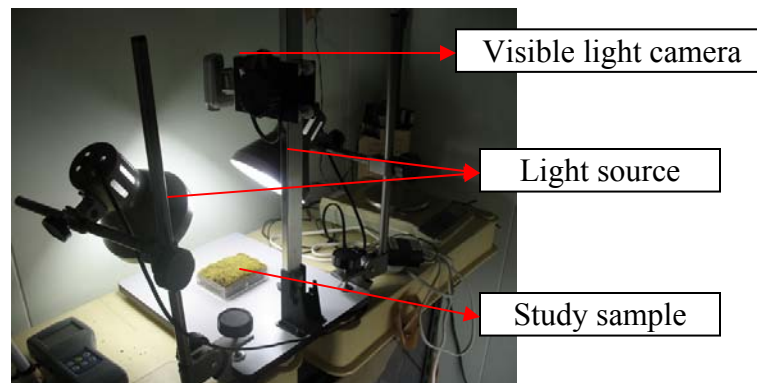


Figure 4. Image acquisition.

### 2.2.1 Colour Features (CF)

The RGB colour space is the default colour space for most available image formats. Any other colour space can be obtained from a linear or non-linear transformation from RGB. RGB is the most commonly used colour space for storing and representing digital images, since the data captured by a camera is normally provided as RGB. RGB correspond to the three primary colours: red, green and blue, respectively. The RGB CF can be described as following (Hendrawan and Murase, 2009):

$$\text{Average red index} = \frac{1}{M} \sum_{i=1}^M \frac{R}{R + G + B} \quad (2)$$

$$\text{Average green index} = \frac{1}{M} \sum_{i=1}^M \frac{G}{R + G + B} \quad (3)$$

$$\text{Average blue index} = \frac{1}{M} \sum_{i=1}^M \frac{B}{R + G + B} \quad (4)$$

$$\text{Red mean value} = \frac{1}{M} \sum_{i=1}^M R \quad (5)$$

$$\text{Green mean value} = \frac{1}{M} \sum_{i=1}^M G \quad (6)$$

$$\text{Blue mean value} = \frac{1}{M} \sum_{i=1}^M B \quad (7)$$

$$\text{Green/red ratio mean value} = \frac{1}{M} \sum_{i=1}^M \frac{G}{R} \quad (8)$$

$$\text{Green/red ratio variance} = \frac{1}{M} \sum_{i=1}^M (x_i - \bar{x})^2 \quad (9)$$

where:  $R$  (red value);  $G$  (green value);  $B$  (blue value);  $M$  is the total number of pixels;  $x_i$  is green/red ratio value and  $\bar{x}$  is green/red ratio mean value.

HSV and HSL colour systems were developed from RGB colour system. These two colour systems are related to each other and approximately to human's concept of tint, shade and tone. Hue is pure colour according to its wavelength, saturation is the amount of the colour with respect to white, and the third axis (called value and lightness respectively) is the amount of light and embodies the achromatic concept of intensity. These spaces have many advantages (Grande *et al.*, 2008). In particular the use of hue for distinguishing features often corresponds to human perception and, what is more important it ignores shading effects. This can be crucial in dealing with granular materials, where shading effects may be dominant, because of the discrete, three-dimensional nature of the particles. The detail conversion method from RGB to HSV and HSL colour spaces can be seen in Angulo and Serra, 2007. Features extracted from HSV and HSL colour systems included hue mean value, saturation<sub>(HSV)</sub> mean value, value<sub>(HSV)</sub> mean value, saturation<sub>(HSL)</sub> mean value and lightness<sub>(HSL)</sub> mean value which are calculated using the same equation as red mean value, green mean value and blue mean value.

### 2.2.2 Morphological Features (MF)

Accurate measurement of green canopy area is special concern to Sunagoke moss due to the relationship with water content. MF included browning index, green canopy index and perimeter index. Browning process on Sunagoke moss can be influenced by virus, fungi, water content or environment condition. The threshold point of browning index and green canopy index can be determined using a combination of RGB colour value and green/red ratio value (Hendrawan and Murase, 2008). Perimeter is used in calculating the border of an object (green canopy area). Water content directly affects changes in green canopy index, perimeter index and browning index (Hendrawan and Murase, 2009). The green canopy, perimeter and browning area were evaluated by pixel count (PC) method as shown in figure 5. The PC method counted the number of pixels in the picture field (Igathianathane *et al.*, 2006).

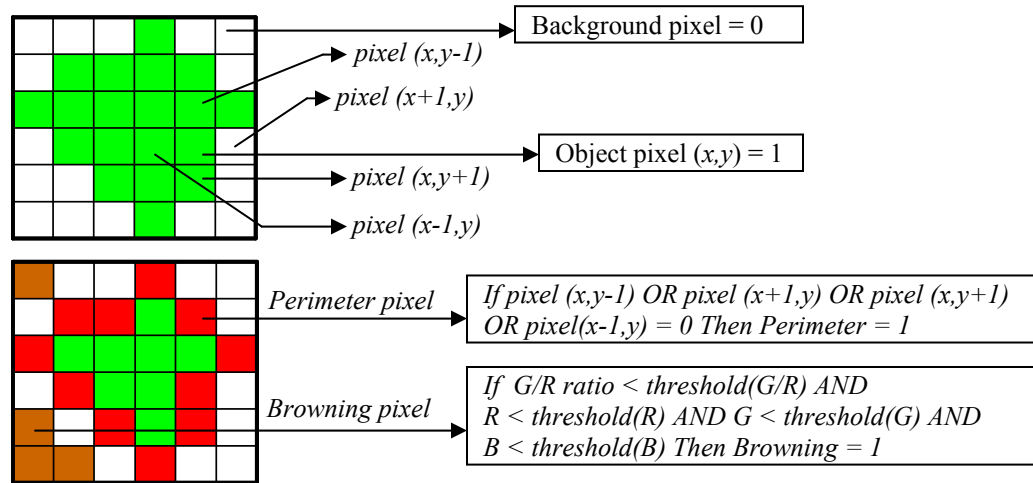


Figure 5 PC method for determining MF.

### 2.2.3 Textural Features (TF)

Texture is a measure of the variation of intensity at scales smaller than the picture field overall scale (Petrou and Sevilla, 2006). Two-dimensional co-occurrence (grey-level dependence) matrices are generally used in texture analysis because they are able to capture the spatial dependence of grey-level values within an image (Haralick *et al.*, 1973). The textural analysis can be considered as one of applicable techniques for extracting image features (Haralick *et al.*, 1973; Murase *et al.*, 1994). Texture has been one of the most important characteristic which have been used to classify and recognize objects and scenes. A 2D co-occurrence matrix,  $P$ , is an  $n \times n$  matrix, where  $n$  is the number of grey-levels within an image. The matrix acts as an accumulator so that  $P[i,j]$  counts the number of pixel pairs having the intensities  $i$  and  $j$ . Pixel pairs are defined by a distance and direction which can be represented by a displacement vector  $d = (dx, dy)$ , where  $dx$  represents the number of pixels moved along the x-axis, and  $dy$  represents the number of pixels moved along the y-axis of an image slice.

The grey colour space involves conversion of RGB images to grey-level images before extraction of the Spatial Grey-Level Dependence Matrices (SGDM) with the equation as following (Ondimu and Murase, 2008):

$$Grey = 0.3 R + 0.59 G + 0.11 B \quad (10)$$

Colour texture analysis as espoused by Colour Co-occurrence Matrix (CCM) method is based on the hypothesis that use of colour features in the visible spectrum provides additional image characteristics over the traditional grey-level representation. Hendrawan and Murase (2009) observed red CCM TF, green CCM TF, blue CCM TF and grey CCM TF for identifying water content. The results showed that combination of angle ( $\theta = 0$ ) and distance ( $d = 1$ ) performed better than the other combination of  $\theta$  and  $d$  to identify water content. Therefore, in this study, TF were extracted at distance ( $d = 1$ ) and angle ( $\theta = 0$ ). The range of red CCM, green CCM, blue CCM, hue CCM, saturation<sub>(HSV)</sub> CCM, value<sub>(HSV)</sub> CCM, saturation<sub>(HSL)</sub> CCM, lightness<sub>(HSL)</sub> CCM and grey CCM within a given image determines the dimensions of a two-dimensional co-occurrence matrix. Each colour space has 256 grey-levels, which makes the co-occurrence matrix 256 x 256. One set of TF consists of ten equations. The following TF were used in this research (Kurani *et al.*, 2004):

$$Entropy = -\sum_i^M \sum_j^N P[i, j] \log P[i, j] \quad (11)$$

$$Energy = \sum_i^M \sum_j^N P^2[i, j] \quad (12)$$

$$Contrast = \sum_i^M \sum_j^N (i - j)^2 P[i, j] \quad (13)$$

$$Homogeneity = \sum_i^M \sum_j^N \frac{P[i, j]}{1 + |i - j|} \quad (14)$$

$$Sum\ Mean = \frac{1}{2} \sum_i^M \sum_j^N (iP[i, j] + jP[i, j]) \quad (15)$$

$$Variance = \frac{1}{2} \sum_i^M \sum_j^N ((i - \mu)^2 P[i, j] + (j - \mu)^2 P[i, j]) \quad (16)$$

$$Correlation = \sum_i^M \sum_j^N \frac{(i - \mu)(j - \mu)P[i, j]}{\sigma^2} \quad (17)$$

$$Maximum\ Probability = \max_{i, j}^{M, N} P[i, j] \quad (18)$$

$$Inverse\ Difference\ Moment = \sum_i^M \sum_j^N \frac{P[i, j]}{|i - j|^k} \quad i \neq j \quad (19)$$

$$Cluster\ Tendency = \sum_i^M \sum_j^N (i + j - 2\mu)^k P[i, j] \quad (20)$$

where:  $P(i, j)$  is the  $(i, j)^{th}$  element of a normalized co-occurrence matrix, and  $\mu$  and  $\sigma$  are the mean and standard deviation of the pixel element given by the following relationships:

$$P[i, j] = \frac{N(i, j)}{M} \quad (21)$$

$$\mu = \sum_i^M i \sum_j^N P[i, j] \quad (22)$$

$$\sigma = \sum_i^M (i - \mu)^2 \sum_j^N P[i, j] \quad (23)$$

where:  $N(i, j)$  is the number counts in the image with pixel intensity  $i$  followed by pixel intensity  $j$  at one pixel displacement to the left, and  $M$  is the total number of pixels.

Based on equations 11 – 20, a total of 90 TF were extracted *i.e.* 10 TF each for grey CCM, red CCM, green CCM, blue CCM, hue CCM, saturation<sub>(HSV)</sub> CCM, saturation<sub>(HSL)</sub> CCM, value<sub>(HSV)</sub> CCM and lightness<sub>(HSL)</sub> CCM.

### 2.2.3 BPNN for prediction

Prediction is common task in many fields. ANN has been shown to be successful as predictive tools in a variety of ways such as predicting the level of some event outcome (Patterson, 1996). In general, ANN is good at learning perceptive type of tasks such as the recognition of complex patterns. Comparative studies made by researchers suggest that ANN compare favourably with conventional statistical pattern recognition methods. A three layers BPNN structure as shown in figure 6 has been developed for predicting Sunagoke moss water content. The number of neurons

in the input layer was determined by the number of input features. Five models of hidden nodes architecture were developed *i.e.* 10, 15, 20, 25 and 30 hidden nodes. The output layer consisted of single neuron. The output was water content corresponding to the input features. The training, validation and testing performance criterion for the prediction was Mean Square Error (MSE) given by equation 24.

$$MSE = \frac{1}{N_n} \sum_{i=1}^{N_n} (S_i - St_i)^2 \quad (24)$$

where  $N_n$  is number of input feature vectors,  $S_i$  is the water content predicted by BPNN model, and  $St_i$  is the target water content determined by equation 1. The 300 samples data of Sunagoko moss were randomized and divided into three parts which were 200 data as training-set, 50 data as validation-set and 50 data as testing-set. The models were trained using BPNN; training was stopped after 400 iterations. Learning rate of 0.5 and momentum of 0.5 were chosen through trial and error.

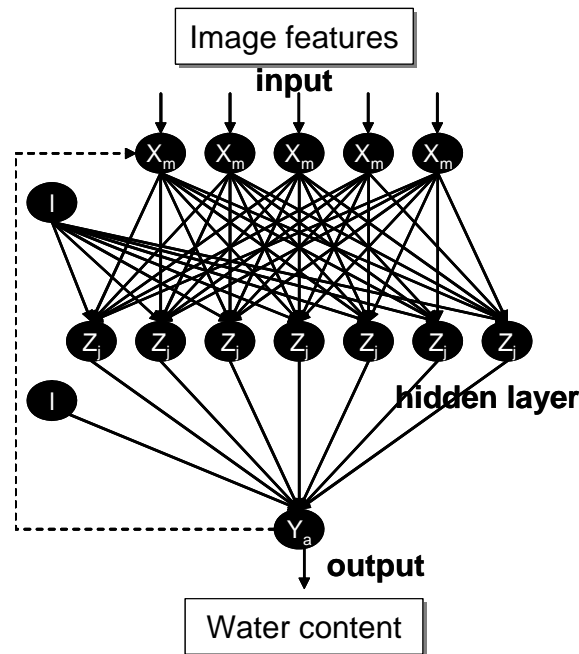


Figure 6. Architecture of three layers Back-Propagation Neural Network.

#### 2.2.4 Neural-GA for optimizing FS

A basic GA, as generally described by Goldberg (1989) and Holland (1975) was used for optimizing FS. GA is search algorithms based on the mechanics of natural selection and natural genetics. In this research, a neural-GA was developed for FS based on the neural network pattern recognition. The objective function in neural-GAs is minimizing validation-set MSE of feature-subset. The steps shown in figure 7 can be described as follows:

1. Generate population randomly in which individuals (number of individuals  $n_i = 50$ ) characterized by chromosomes represent a set of possible solutions (e.g.  $ga_j: 0,1,1,0,0,0,0,1,0,0,1,0, \dots, m$ ), where  $m$  is the number of total features which equals to 106 features. The chromosome defined contains 106 genes, one gene for each feature, which can take 2 values. A value of 0 indicates that the corresponding feature is not selected, and the value 1 means that the feature is selected.

2. Compute the fitness function which reflects the degree of goodness of the individuals for the problem and evaluate the fitness of all individuals of the population by using BPNN. The fitness of the chromosome is calculated according to the prediction rate (validation-set MSE) of the evolved subset of features.
3. Select the fittest individuals to be parents for reproducing offspring using roulette wheel selection strategy.
4. Create offspring with two points crossover and mutation operators by changing the selected individuals during the mating periods. Two points crossover (point1 and point2) are selected randomly, where  $\text{point1} < \text{point2}$ , and  $\text{point1} > 1$ ,  $\text{point2} < m$ .
5. Displace the parents with good offspring to compose the subsequent generation according to probability best chromosome which is set to 0.2.
6. Stopping criterion. The search will terminate if the iteration has reached 500 iterations. Individual with the best fitness in the last population is considered to be the optimal individual.

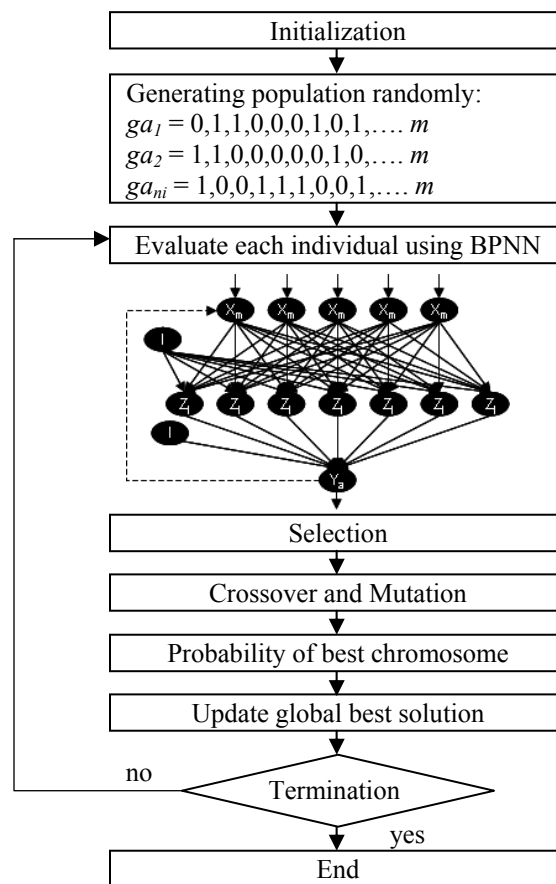


Figure 7 Neural-GA for feature selection.

### 2.2.5 Neural-ACO for optimizing FS

ACO was initially proposed by Coloni, Dorigo and Maniezzo (Dorigo and Stutzle, 2004). ACO was inspired by the foraging behaviour of real ants. The main underlying idea was that of parallelizing search over several constructive computational threads, all based on a dynamic memory structure incorporating information on the effectiveness of previously obtained results

and in which the behaviour of each single agent is inspired by the behaviour of real ants. The steps of neural-ACO shown in figure 8 can be described as follows:

1. Set the initial parameters i.e. the number of ant ( $na$ ) population ( $a_1, a_2, a_3, \dots, a_{na}$ ) in which  $na = 50$ ; global iterations = 500; heuristic ( $\eta_{i\psi}$ ) which is defined as the inverse of the validation MSE between two features ( $i, \psi$ ) as the input of BPNN; intensity of pheromone trail level ( $\tau = 100$ ); the best selected ants ( $k = 8$ ); pheromone constant ( $\alpha = 1$ ); heuristic constant ( $\beta = 1$ ) and evaporation rate of pheromone  $\rho[0, 1]$ .
2. Generating ants for solution generation. At the first iteration, assign any ant randomly to one feature and visiting features, each ant builds solutions completely. For the next iterations, each ant movement for finding the trail path is based on the pheromone and heuristic probability. For ant  $a$ , the probability  $p_{i\psi}$  of moving from state  $i$  to state  $\psi$  depends on the combination of two values i.e. the heuristic  $\eta$  of the move and the pheromone trail level  $\tau$  of the move. Probabilities are computed as follows:  $p_{i\psi}$  is equal to 0 for all moves which are infeasible, otherwise it is computed by means of the following formula, where  $\alpha$  and  $\beta$  is a user-defined parameter ( $0 < \alpha < 1$ ;  $0 < \beta < 1$ ). Parameter  $\alpha$  and  $\beta$  control the relative importance of the trail and the attractiveness, respectively.

$$p_{i\psi}^a = \frac{\tau_{i\psi}^\alpha \cdot \eta_{i\psi}^\beta}{\sum_{a \in allowed_a} (\tau_{i\psi}^\alpha \cdot \eta_{i\psi}^\beta)} \quad (25)$$

If an ant is not able to decrease the validation-set MSE in ten successive steps, it will finish its work and exit. Each ant consist of feature-subset with selected features as ant paths (e.g.  $a_i: 0,1,1,0,0,0,0,1,0,0,1,0, \dots, m$ ), where  $m$  is the number of total features which equals to 106 features. Each ant in the population represents a candidate solution to the feature subset selection problem. A value of 0 indicates that the corresponding feature is not selected and will not be added as the input of BPNN, while a value of 1 means that the feature is selected and will be added as the input of BPNN.

3. Evaluation of ants ( $a$ ). Evaluate ants (feature-subsets) using BPNN. Each ant solution ( $T^{ant}$ ) is calculated according to the prediction rate (validation MSE) of the evolved subset of features. The values of the BPNN inputs are the feature-subsets. One output of BPNN is the solution for determining water content of Sunagoke moss.
4. Update the global best solution ( $T^{best}$ ) by the current ant solution ( $T^{ant}$ ). The objective function is minimizing validation MSE of BPNN.

$$T^{best} \begin{cases} T^{best} & \text{if } q(T^{best}) \geq q(T^{ant}) \\ T^{ant} & \text{otherwise} \end{cases} \quad (26)$$

5. Pheromone updating. An iteration is defined here as the interval in ( $t, t+I$ ) where each of the ant moves once. We then define an epoch to be every  $n$  iterations, when each ant has completed a tour. After each epoch the pheromone trails intensity are updated according to the following formula:

$$\tau_{i\psi}(t+n) = (1-\rho)\tau_{i\psi}(t) + \sum_{a=1}^k \Delta\tau_{i\psi} \quad (27)$$

where  $\Delta\tau_{i\psi}$  represents the sum of the contributions of all best  $k$  ants that used move ( $i, \psi$ ) to construct their solution between time  $t$  and  $t+I$ . Using the feature subsets of the best  $k$  ants, the pheromone trails intensity are updated using the following equation:

For  $j = 1$  to  $k$

$$\Delta\tau_{i\psi} = \frac{\max_{g=1:k}(MSE_g) - MSE_j}{\max_{h=1:k}(\max_{g=1:k}(MSE_g) - MSE_h)} \quad (28)$$

In the first iteration, each ant will randomly choose a feature subset of  $m$  features. Only the best  $k$  subsets,  $k < na$ , will be used to update the pheromone trail and influence the feature subsets of the next iteration. In the second and following iterations, each ant will start with  $m-e$  features that are randomly chosen from the previously selected  $k$ -best subsets, where  $e$  is an integer that ranges between 1 and  $m-1$ .

6. Generation of new ants. In this step previous ants are removed and new ants are generated.
7. Stopping criterion: the algorithm stops with the total-best solution  $T^{TB}$ . The search will terminate if the global iteration has been reached.

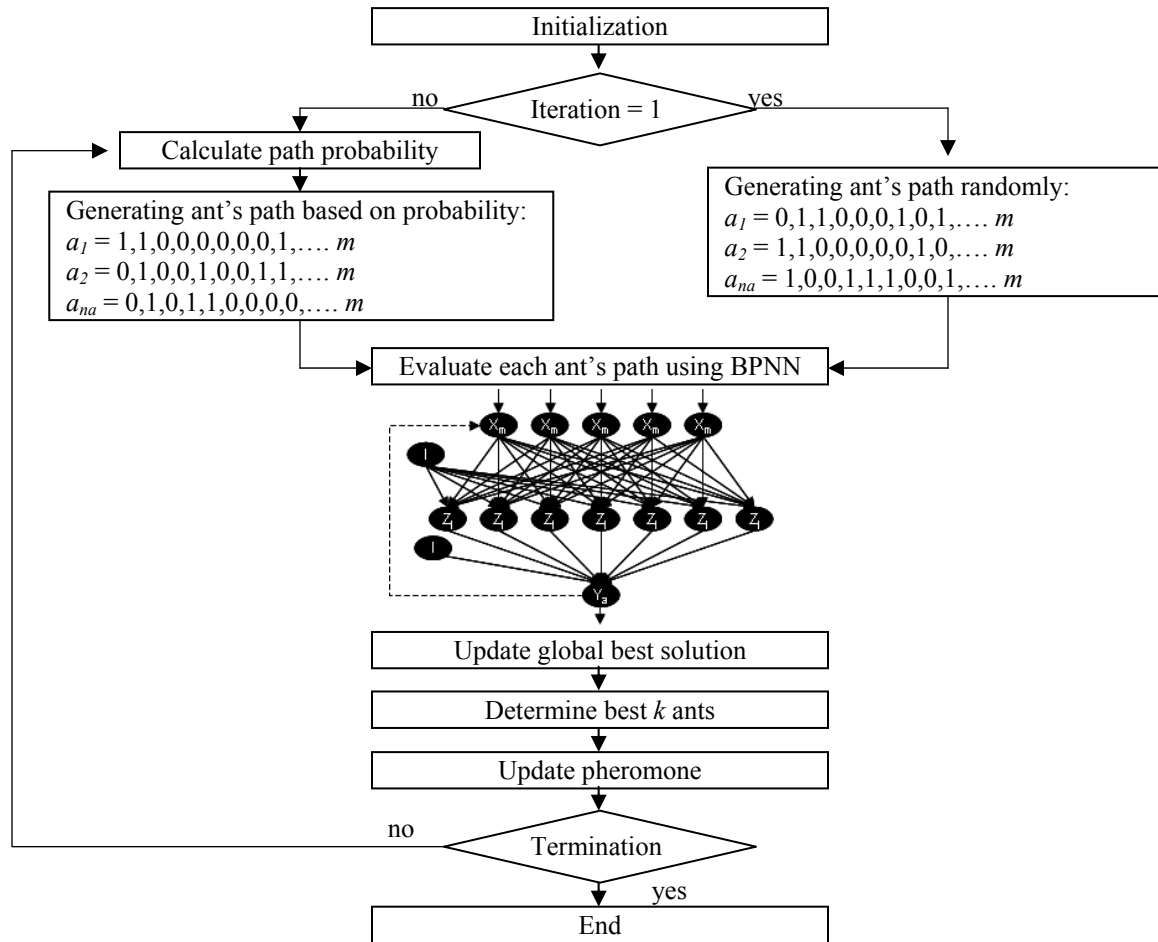


Figure 8. Neural-ACO for feature selection.

### 3. RESULTS AND DISCUSSION

#### 3.1 Water content and image features

Figure 9 shows the changes in Sunagoke moss appearance due to drying process in ten days experiment. Drying process in Sunagoke moss was affected by evapotranspiration process. Hendrawan and Murase (2009) mentioned that evapotranspiration was much higher when the

moss layer is wet. The graph shows that moss at high water condition has faster drying rate than moss at low water condition. The evapotranspiration process is composed of evaporation and transpiration. Water content has a linear correlation with evapotranspiration. It means that as water content increases, the evapotranspiration rate also increases.

Visible light photography has been effective in determining the percentage of maximal net CO<sub>2</sub> uptake of plant using green/red ratio (Graham *et al.*, 2006). Red referred to a broad band of wavelengths (600-699 nm) and green to a broad band of wavelengths (500-599 nm). During the photosynthesis process, plant absorbs red wavelengths that makes it reflect red wavelengths less than green wavelengths. The more it absorbs red wavelengths the higher the green/red ratio value. Because photosynthesis has correlation with water existence, the changes of green and red wavelengths reflection can be used as indicators of the water existence in plant. If Sunagoke moss does not have enough water or it has too much water, then photosynthesis process will not be optimum. Photosynthesis of Sunagoke moss will be optimum if it has appropriate water content condition. The optimal water content based on photosynthesis rate (light in the environment growth condition: 100  $\mu\text{mol m}^{-2}\text{s}^{-1}$ ) was between 2.0 – 3.0  $\text{gg}^{-1}$  (Hendrawan and Murase, 2009).

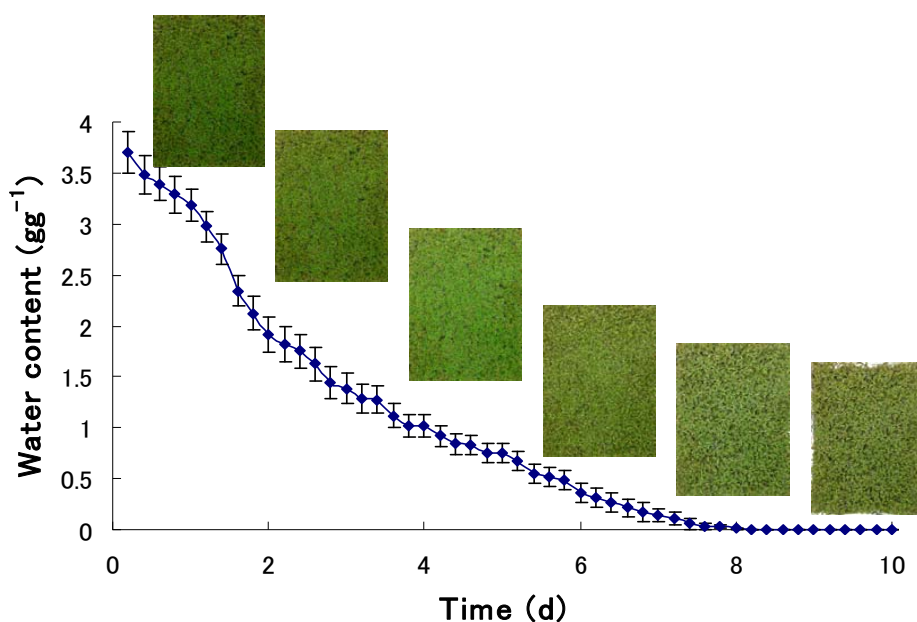
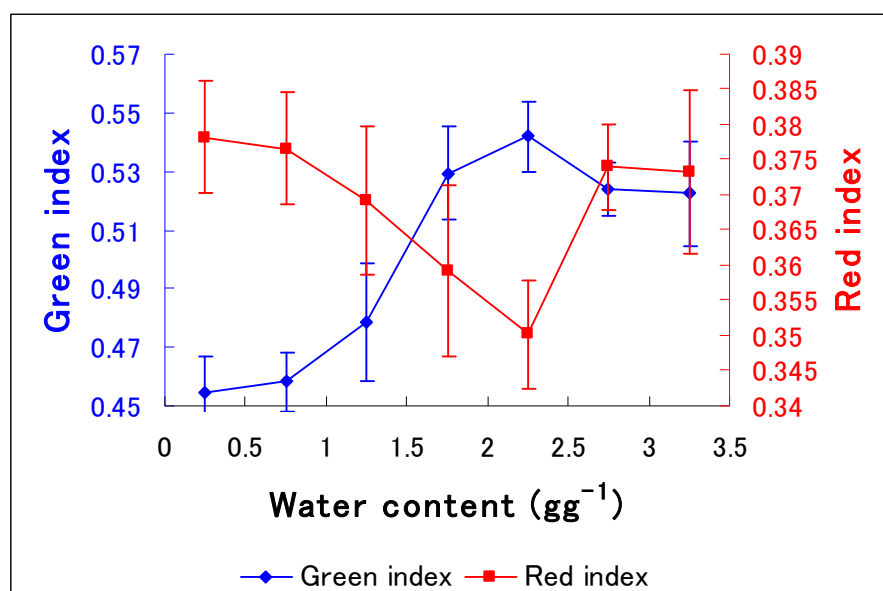
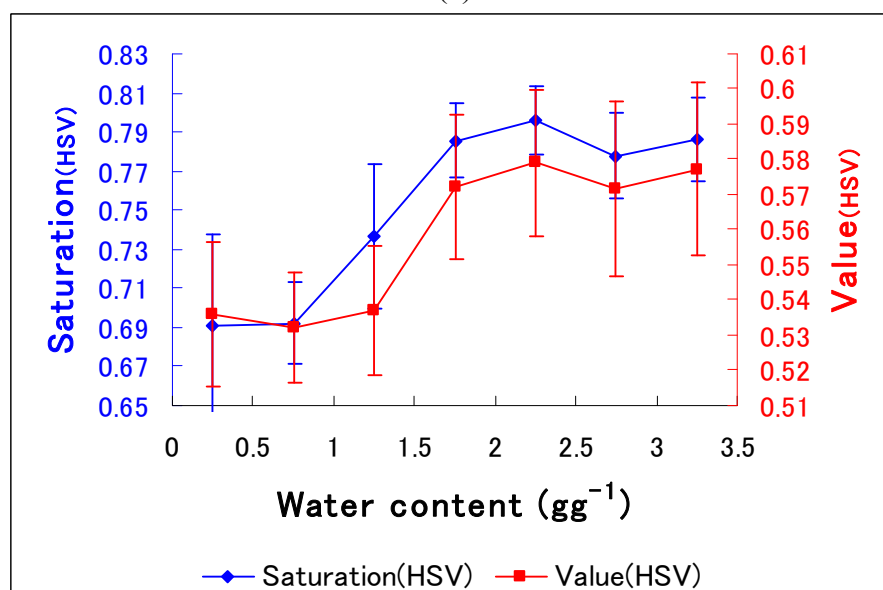


Figure 9. Changes in Sunagoke moss appearance due to drying process.

Figure 10 shows the relationships of Sunagoke moss water content and CF. In dry condition, CF such as average green index,  $\text{saturation}_{(\text{HSV})}$  mean value and  $\text{value}_{(\text{HSV})}$  mean value were low, they increased gradually until the water content was between 2.0 - 2.5  $\text{gg}^{-1}$ . In water content above 2.5  $\text{gg}^{-1}$  they decreased and remained fairly stable after the water content reached 2.75  $\text{gg}^{-1}$ . This was reversed for average red index.



(a)



(b)

Figure 10. Sunagoke moss water content and CF: (a) average green index and average red index; (b) saturation<sub>(HSV)</sub> mean value and value<sub>(HSV)</sub> mean value.

Figure 11 shows the relationships of Sunagoke moss water content and MF. It shows that water content affects to the browning process of Sunagoke moss. In dry condition, browning index was high, it decreased gradually until the water condition between 2.0 - 2.5  $\text{gg}^{-1}$ , it remained fairly stable there after. This was reversed for green canopy index. Figure 12 shows the relationships of Sunagoke moss water content and TF. In dry condition, TF such as green CCM energy, saturation<sub>(HSL)</sub> CCM homogeneity, saturation<sub>(HSL)</sub> CCM maximum probability, saturation<sub>(HSV)</sub> CCM energy and saturation<sub>(HSV)</sub> CCM maximum probability increased up to 2.0 - 2.5  $\text{gg}^{-1}$  of water content and remained fairly stable there after. This was reversed for green CCM entropy which showed a decreasing trend of values and reached the lowest value when the water condition was between 2.0 - 2.5  $\text{gg}^{-1}$ . Hence optimum water content of Sunagoke moss based on

CF, MF and TF can be achieved between 2.0 - 2.5  $\text{gg}^{-1}$ . When the *P*-value (significant level) in Table 1 is less than 0.01, there is a significant difference between groups with a confidence level of 99%. According to this rule, average green index, average red index, saturation<sub>(HSV)</sub> mean value, value<sub>(HSV)</sub> mean value, browning index, green canopy index, green CCM entropy, green CCM energy, saturation<sub>(HSL)</sub> CCM homogeneity, saturation<sub>(HSL)</sub> CCM maximum probability, saturation<sub>(HSV)</sub> CCM energy and saturation<sub>(HSV)</sub> CCM maximum probability as shown in figure 10 to 12 were significantly different from each other.

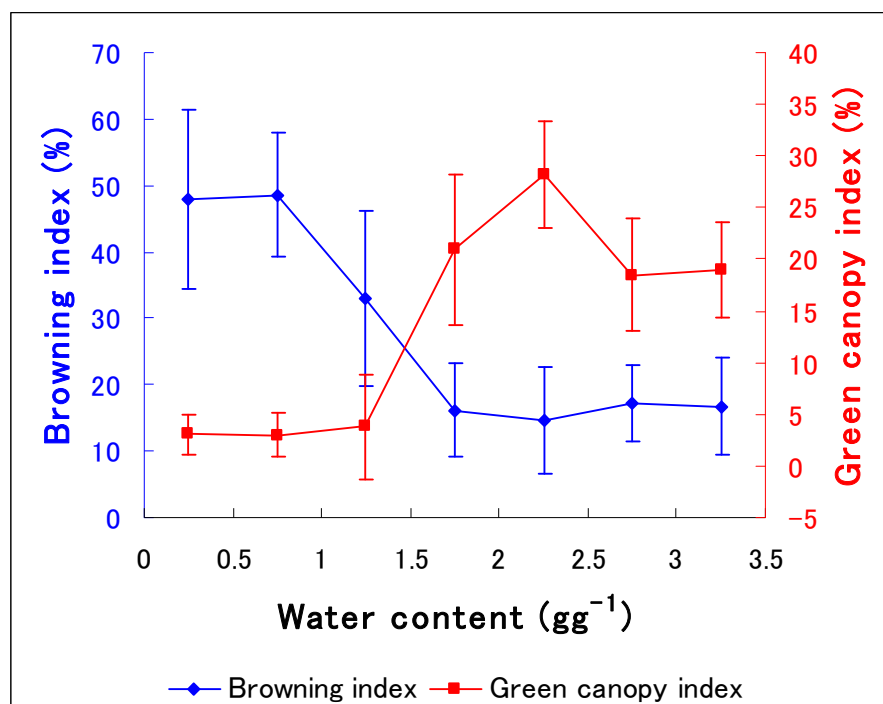
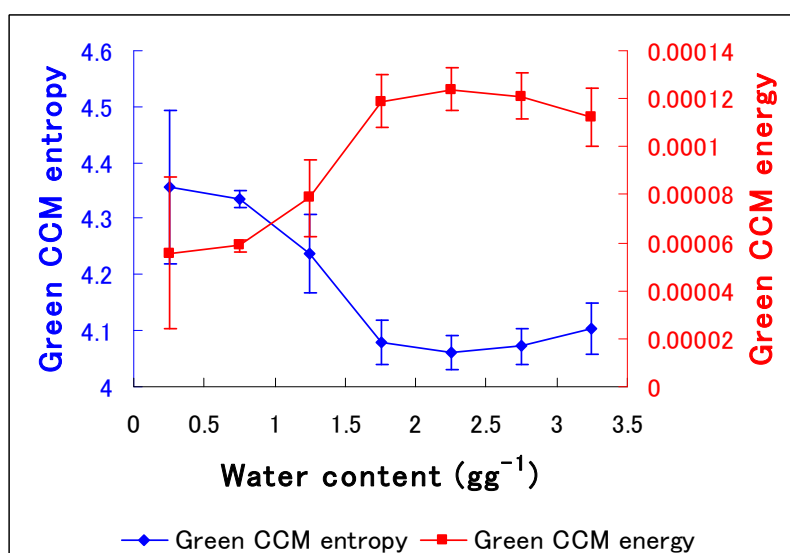
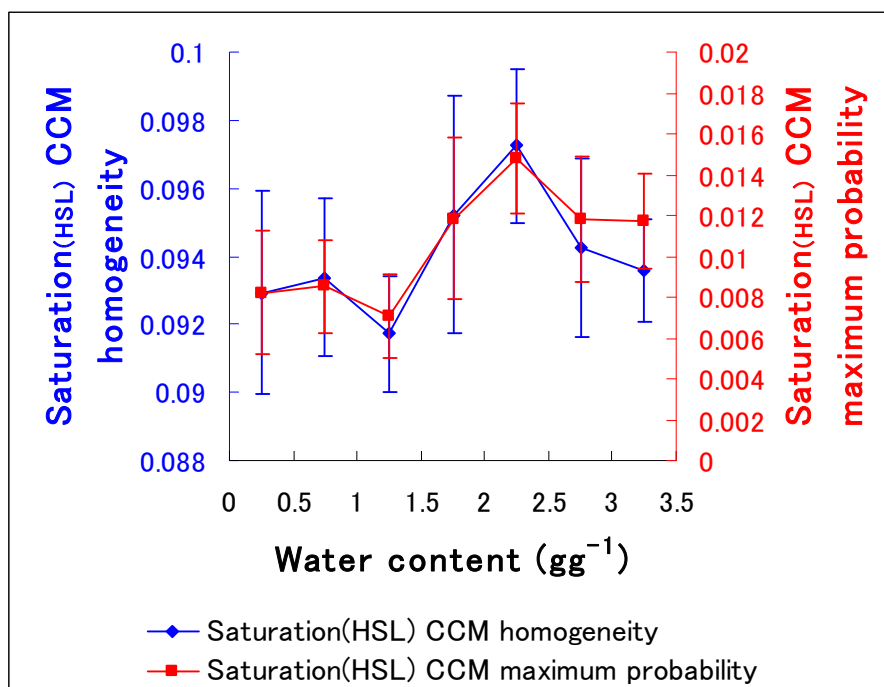


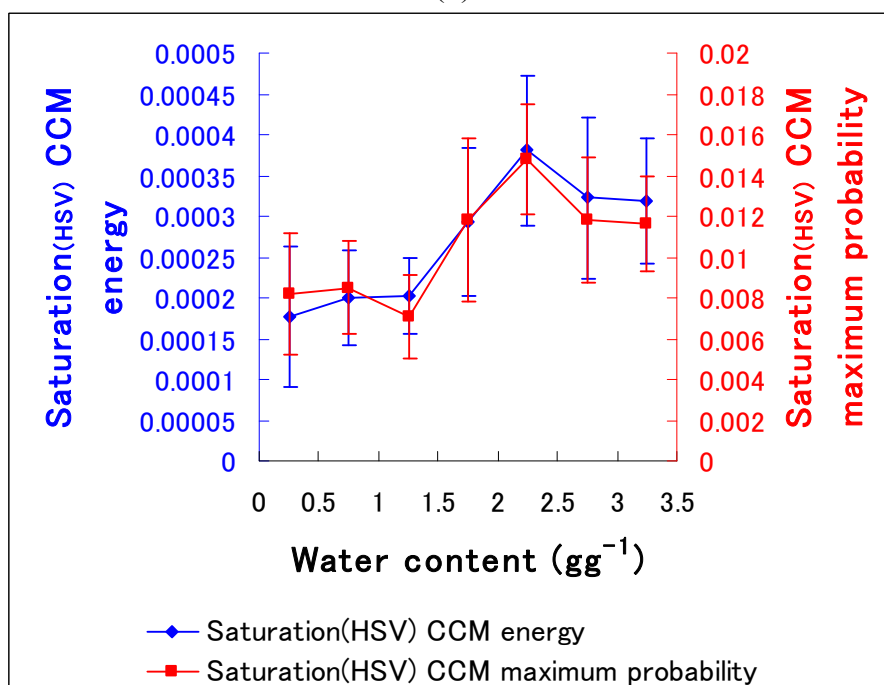
Figure 11. Sunagoko moss water content and MF (browning index and green canopy index).



(a)



(b)



(c)

Figure 12. Sunagoko moss water content and TF: (a) RGB CCM TF (green CCM entropy and green CCM energy); (b) HSL CCM TF (saturation<sub>(HSL)</sub> CCM homogeneity and saturation<sub>(HSL)</sub> CCM maximum probability); (c) HSV CCM TF (saturation<sub>(HSV)</sub> CCM energy and saturation<sub>(HSV)</sub> CCM maximum probability).

Table 1 One way ANOVA results

Parameters	Relation	SS	df	MS	F	P-value	F-crit.
average green index	Between group	0.0814	6	0.0135	50.8077	2.75x10 <sup>-22</sup>	3.1027
	Within group	0.0168	63	2.67x10 <sup>-4</sup>			
	Total	0.0982	69				
average red index	Between group	0.0057	6	0.0009	11.6751	9.45x10 <sup>-9</sup>	3.1027
	Within group	0.0052	63	8.24x10 <sup>-5</sup>			
	Total	0.0109	69				
saturation <sub>(HSV)</sub> mean value	Between group	0.1146	6	0.0191	24.3033	1.10x10 <sup>-14</sup>	3.1027
	Within group	0.0495	63	7.86x10 <sup>-4</sup>			
	Total	0.1641	69				
value <sub>(HSV)</sub> mean value	Between group	0.0261	6	0.0043	10.6234	4.01x10 <sup>-8</sup>	3.1027
	Within group	0.0257	63	4.09x10 <sup>-4</sup>			
	Total	0.0518	69				
browning index	Between group	13953.3	6	2325.54	25.4081	4.22x10 <sup>-15</sup>	3.1027
	Within group	5766.24	63	91.5276			
	Total	19719.5	69				
green canopy index	Between group	6233.44	6	1038.91	42.7911	2.14x10 <sup>-20</sup>	3.1027
	Within group	1529.54	63	24.2785			
	Total	7762.99	69				
green CCM entropy	Between group	0.9804	6	0.1634	136.8163	3.48x10 <sup>-34</sup>	3.1027
	Within group	0.0752	63	0.00119			
	Total	1.0557	69				
green CCM energy	Between group	5.33x10 <sup>-8</sup>	6	8.89x10 <sup>-9</sup>	101.9301	1.65x10 <sup>-30</sup>	3.1027
	Within group	5.50x10 <sup>-9</sup>	63	8.72x10 <sup>-11</sup>			
	Total	5.88x10 <sup>-8</sup>	69				
saturation <sub>(HSL)</sub> CCM homogeneity	Between group	2.89x10 <sup>-4</sup>	6	4.82x10 <sup>-5</sup>	9.1911	3.18x10 <sup>-7</sup>	3.1027
	Within group	3.30x10 <sup>-4</sup>	63	5.24x10 <sup>-6</sup>			
	Total	6.19x10 <sup>-4</sup>	69				
saturation <sub>(HSL)</sub> CCM max. probability	Between group	5.80x10 <sup>-4</sup>	6	9.67x10 <sup>-5</sup>	22.2945	6.81x10 <sup>-14</sup>	3.1027
	Within group	2.73x10 <sup>-4</sup>	63	4.34x10 <sup>-6</sup>			
	Total	8.53x10 <sup>-4</sup>	69				
saturation <sub>(HSV)</sub> CCM energy	Between group	3.64x10 <sup>-7</sup>	6	6.06x10 <sup>-8</sup>	15.0593	1.33x10 <sup>-10</sup>	3.1027
	Within group	2.54x10 <sup>-7</sup>	63	4.02x10 <sup>-9</sup>			
	Total	6.17x10 <sup>-7</sup>	69				
saturation <sub>(HSV)</sub> CCM max. probability	Between group	5.86x10 <sup>-4</sup>	6	9.76x10 <sup>-5</sup>	22.4539	5.87x10 <sup>-14</sup>	3.1027
	Within group	2.74x10 <sup>-4</sup>	63	4.35x10 <sup>-6</sup>			
	Total	8.60x10 <sup>-4</sup>	69				

where SS = Sum of Squares; MS = Mean Square; *F-crit.* = F critical

### 3.2 Water content prediction using BPNN

BPNN model performance was tested successfully to describe the relationship between Sunagoke moss water content and image features. Figure 13 shows water content prediction using BPNN based on average validation MSE with the inputs of individual feature-subsets (CF, MF, grey CCM TF, red CCM TF, green CCM TF, blue CCM TF, hue CCM TF, saturation<sub>(HSV)</sub> CCM TF, value<sub>(HSV)</sub> CCM TF, saturation<sub>(HSL)</sub> CCM TF and lightness<sub>(HSL)</sub> CCM TF) in different hidden nodes number. From figure 13, we can see that MF has the lowest average validation MSE when using 30 hidden nodes.

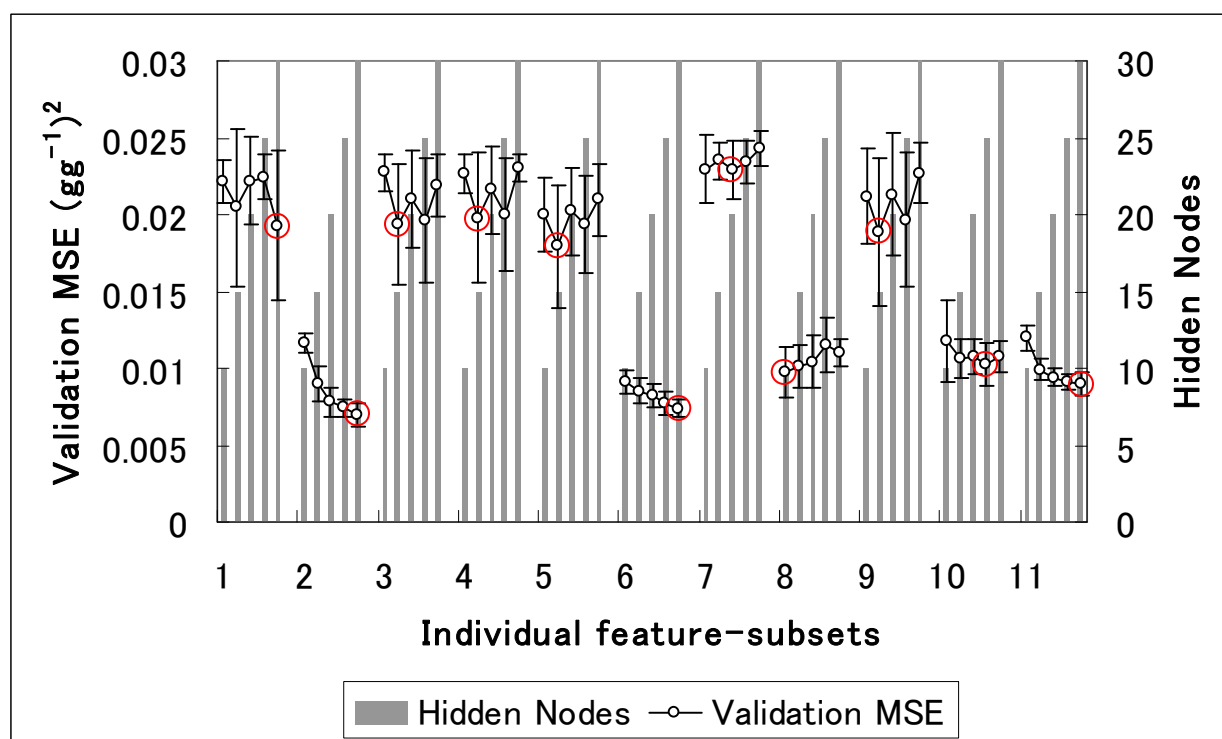


Figure 13 Average validation MSE of each individual feature-subset with different number of hidden nodes: (1) CF; (2) MF; (3) grey CCM TF; (4) red CCM TF; (5) green CCM TF; (6) blue CCM TF; (7) hue CCM TF; (8) saturation<sub>(HSV)</sub> CCM TF; (9) value<sub>(HSV)</sub> CCM TF; (10) saturation<sub>(HSL)</sub> CCM TF; (11) lightness<sub>(HSL)</sub> CCM TF.

Table 2 shows the overall prediction results using the best selected number of hidden nodes in BPNN. It shows that most of the TF (grey CCM TF, red CCM TF, green CCM TF, blue CCM TF, saturation<sub>(HSV)</sub> CCM TF, value<sub>(HSV)</sub> CCM TF, saturation<sub>(HSL)</sub> CCM TF and lightness<sub>(HSL)</sub> CCM TF) had lower training MSE than CF and MF. The saturation<sub>(HSV)</sub> CCM TF had the lowest training MSE of  $7.80 \times 10^{-3} \text{ (gg}^{-1}\text{)}^2$ . MF had lowest validation MSE than other models. The hue CCM TF had the highest training and validation MSE. The training MSE of BPNN models less than 1% were obtained. It can be said that the performance of BPNN models is satisfactory as shown in Table 2. In general, training of BPNN may be terminated at the convergence with total training MSE value less than 1% (Patterson, 1996). Table 3 shows that the significant level is less than 0.01, which means there is a significant difference between the groups of training-set MSE, validation-set MSE and testing-set MSE with a confident level of 99%.

All models showed negligible absolute deviation in predicting the water content for ten iterations. Based on the average of training, validation and testing, lightness<sub>(HSL)</sub> CCM TF showed the lower absolute deviation, followed by saturation<sub>(HSV)</sub> CCM TF, hue CCM TF, MF, blue CCM TF, saturation<sub>(HSL)</sub> CCM TF, red CCM TF, grey CCM TF, green CCM TF, value<sub>(HSV)</sub> CCM TF and CF in that order, respectively. It means that lightness<sub>(HSL)</sub> CCM TF showed the highest consistency and highest reliability in predicting water content in Sunagoke moss. On the other hand, CF showed the least consistency. The validation results show that BPNN model using MF as the inputs had the best performance to predict water content with the validation MSE of  $6.70 \times 10^{-3} \text{ (gg}^{-1}\text{)}^2$  followed by blue CCM TF, lightness<sub>(HSL)</sub> CCM TF, saturation<sub>(HSV)</sub> CCM TF,

saturation<sub>(HSL)</sub> CCM TF, value<sub>(HSV)</sub> CCM TF, green CCM TF, grey CCM TF, red CCM TF, CF and hue CCM TF in that order, respectively.

Table 2. Performance of water content prediction using BPNN

BPNN Model	Average Mean Square Error ( $gg^{-1}$ ) <sup>2</sup>					
	Training-set		Validation-set		Testing-set	
	Mean	Deviation (abs.)	Mean	Deviation (abs.)	Mean	Deviation (abs.)
CF	$1.41 \times 10^{-2}$	$1.81 \times 10^{-3}$	$1.74 \times 10^{-2}$	$4.68 \times 10^{-3}$	$7.89 \times 10^{-3}$	$1.50 \times 10^{-3}$
MF	$1.44 \times 10^{-2}$	$1.24 \times 10^{-3}$	$6.70 \times 10^{-3}$	$5.95 \times 10^{-4}$	$7.35 \times 10^{-3}$	$1.18 \times 10^{-3}$
grey CCM TF	$1.31 \times 10^{-2}$	$8.00 \times 10^{-4}$	$1.60 \times 10^{-2}$	$2.95 \times 10^{-3}$	$6.19 \times 10^{-3}$	$1.26 \times 10^{-3}$
<i>r</i> CCM TF	$1.39 \times 10^{-2}$	$9.89 \times 10^{-4}$	$1.68 \times 10^{-2}$	$3.14 \times 10^{-3}$	$4.47 \times 10^{-3}$	$6.82 \times 10^{-4}$
<i>g</i> CCM TF	$1.28 \times 10^{-2}$	$9.38 \times 10^{-4}$	$1.53 \times 10^{-2}$	$3.46 \times 10^{-3}$	$5.09 \times 10^{-3}$	$1.09 \times 10^{-3}$
<i>b</i> CCM TF	$8.59 \times 10^{-3}$	$3.00 \times 10^{-4}$	$7.07 \times 10^{-3}$	$5.59 \times 10^{-4}$	$8.98 \times 10^{-3}$	$2.37 \times 10^{-3}$
<i>h</i> CCM TF	$1.83 \times 10^{-2}$	$5.67 \times 10^{-4}$	$2.13 \times 10^{-2}$	$8.76 \times 10^{-4}$	$3.46 \times 10^{-3}$	$1.24 \times 10^{-3}$
<i>s</i> <sub>(HSV)</sub> CCM TF	$7.80 \times 10^{-3}$	$2.86 \times 10^{-4}$	$8.73 \times 10^{-3}$	$8.64 \times 10^{-4}$	$4.15 \times 10^{-3}$	$8.15 \times 10^{-4}$
<i>v</i> <sub>(HSV)</sub> CCM TF	$1.30 \times 10^{-2}$	$1.07 \times 10^{-3}$	$1.46 \times 10^{-2}$	$3.88 \times 10^{-3}$	$4.23 \times 10^{-3}$	$7.73 \times 10^{-4}$
<i>s</i> <sub>(HSL)</sub> CCM TF	$1.02 \times 10^{-2}$	$6.11 \times 10^{-4}$	$9.24 \times 10^{-3}$	$6.83 \times 10^{-4}$	$8.31 \times 10^{-3}$	$2.28 \times 10^{-3}$
<i>l</i> <sub>(HSL)</sub> CCM TF	$7.91 \times 10^{-3}$	$3.99 \times 10^{-4}$	$8.63 \times 10^{-3}$	$5.01 \times 10^{-4}$	$6.82 \times 10^{-3}$	$5.73 \times 10^{-4}$

where *r* = red, *g* = green, *b* = blue, *h* = hue, *s*<sub>(HSV)</sub> = saturation<sub>(HSV)</sub>, *v*<sub>(HSV)</sub> = value<sub>(HSV)</sub>, *s*<sub>(HSL)</sub> = saturation<sub>(HSL)</sub> and *l*<sub>(HSL)</sub> = lightness<sub>(HSL)</sub>

Table 3. One way ANOVA results

Parameters	Relation	SS	df	MS	<i>F</i>	P-value	<i>F-crit.</i>
Training-set	Between group	$1.05 \times 10^{-3}$	10	$1.05 \times 10^{-4}$	121.703	$5.38 \times 10^{-51}$	2.5052
	Within group	$8.54 \times 10^{-5}$	99	$8.62 \times 10^{-7}$			
	Total	$1.13 \times 10^{-3}$	109				
Validation-set	Between group	$2.46 \times 10^{-4}$	10	$2.46 \times 10^{-4}$	38.46	$9.91 \times 10^{-30}$	2.5052
	Within group	$6.34 \times 10^{-4}$	99	$6.41 \times 10^{-6}$			
	Total	$3.09 \times 10^{-3}$	109				
Testing-set	Between group	$3.64 \times 10^{-4}$	10	$3.64 \times 10^{-5}$	19.2275	$3.81 \times 10^{-19}$	2.5052
	Within group	$1.88 \times 10^{-4}$	99	$1.90 \times 10^{-6}$			
	Total	$5.52 \times 10^{-4}$	109				

where SS = Sum of Squares; MS = Mean Square; *F-crit.* = F critical

Figure 14 shows comparison analysis of validation MSE on each BPNN model which included CF, MF, grey CCM TF, combination of all RGB CCM TF (red CCM TF; green CCM TF; blue CCM TF), combination of all HSV CCM TF (hue CCM TF; saturation<sub>(HSV)</sub> CCM TF; value<sub>(HSV)</sub> CCM TF), combination of all HSL CCM TF (hue CCM TF; saturation<sub>(HSL)</sub> CCM TF; lightness<sub>(HSL)</sub> CCM TF) and combination of all features. Table 4 shows one way ANOVA results which explains the significant difference in figure 14. When the significant level in Table 4 is less than 0.01, there is a significant difference between the groups with a confidence level of 99%. Based on the average validation results show that BPNN model using MF had the highest performance to predict water content followed by combination of all HSV CCM TF, HSL CCM TF, RGB CCM TF, grey CCM TF and CF in that order, respectively. However, based on partial analysis using *t-test*, the results show that there is no significant difference between MF and HSV CCM TF and also no significant difference between MF and HSL CCM TF, but there is a significant difference between MF and other BPNN models (CF, grey CCM TF, RGB CCM TF and all features) at  $\alpha = 0.01$  significant level. HSV CCM TF and HSL CCM TF also have significant difference with other BPNN models (CF, grey CCM TF, RGB CCM TF and all

features). From this analysis we can conclude that MF, HSV CCM TF and HSL CCM TF are recommended as individual feature-subset to be used for predicting water content using BPNN with the average validation MSE of  $6.70 \times 10^{-3} (\text{gg}^{-1})^2$ ,  $6.76 \times 10^{-3} (\text{gg}^{-1})^2$  and  $7.10 \times 10^{-3} (\text{gg}^{-1})^2$  in that order, respectively.

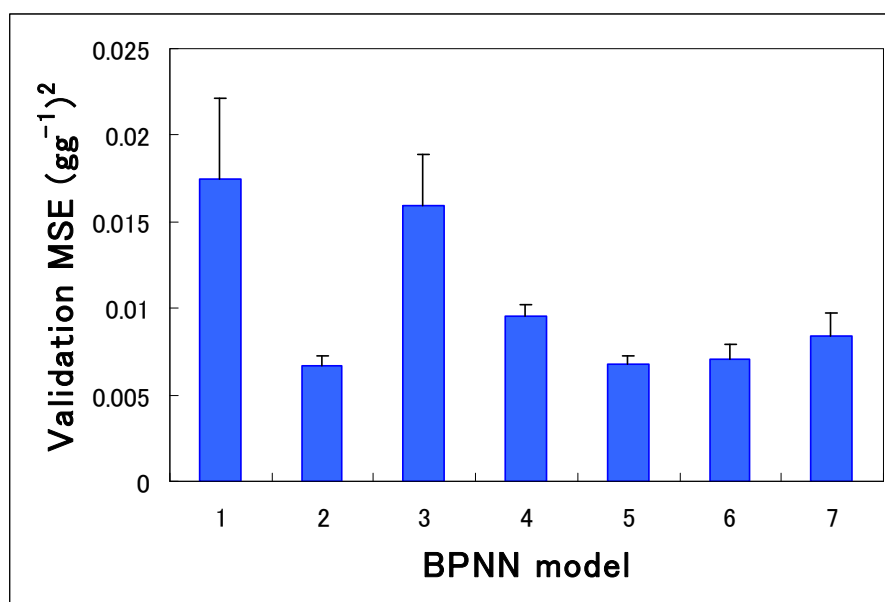


Figure 14. Comparison of validation-set MSE on each BPNN model: (1) CF; (2) MF; (3) grey CCM TF; (4) RGB CCM TF; (5) HSV CCM TF; (6) HSL CCM TF; (7) All features.

Table 4 One way ANOVA results

Relation	SS	df	MS	<i>F</i>	P-value	<i>F-crit.</i>
Between group	$1.22 \times 10^{-3}$	6	$2.04 \times 10^{-4}$	41.7606	$3.91 \times 10^{-20}$	3.1027
Within group	$3.08 \times 10^{-4}$	63	$4.89 \times 10^{-6}$			
Total	$1.53 \times 10^{-3}$	69				

where SS = Sum of Squares; MS = Mean Square; *F-crit.* = F critical

One individual feature-subset stand alone might not be significant for the prediction but might be very significant if combined with other features. FS techniques (neural-GA and neural-ACO) were used to select relevant image features to predict water content.

### 3.3 Neural-GA

GA for FS involve many generations. In each generation, evaluation of an individual (a feature-subset) involves training neural networks. The chromosome contains 106 genes, one gene for each feature, which can take two values. A value of 0 indicates that the corresponding feature is not selected, while a value of 1 means that the feature is selected. An initial population of chromosomes is randomly generated. Crossover process in GA was conducted using two points crossover. Two points were selected randomly. Mutation process was also conducted randomly. Some best chromosomes were kept to be used in the next generation. The roulette wheel selection strategy was used in the algorithm. The application of genetic operators to population members is determined by their fitness (how good a feature-subset is with respect to an

evaluation strategy). Better feature-subsets have a great chance of being selected to form a new subset through crossover or mutation. The research was conducted by the prediction rate based on validation MSE to calculate the fitness for reproduction of GA. The parameter settings for GA include population size: 50; probability of best chromosomes: 0.2; probability of crossover (PC): 0.8 and 0.5; probability of mutation (PM): 0.1 and 0.01; and number of generation was developed until the fitness function converged or 500 generations. Table 5 describes the performance of water content prediction using neural-GA. The combination of PC = 0.8 and PM = 0.1 had the lowest validation MSE ( $3.54 \times 10^{-3} \text{ (gg}^{-1}\text{)}^2$ ) on predicting water content of Sunagoke moss. Neural-GA was also able to reduce irrelevant features and decrease the features from 106 to 47 features.

Table 5. Performance of water content prediction using neural-GA

GA parameter	Number of Selected Features	Mean Square Error ( $\text{gg}^{-1}$ ) <sup>2</sup>		
		Training-set	Validation-set	Testing-set
PC: 0.8; PM: 0.1	47	$3.46 \times 10^{-3}$	$3.54 \times 10^{-3}$	$6.67 \times 10^{-3}$
PC: 0.5; PM: 0.1	52	$3.94 \times 10^{-3}$	$4.58 \times 10^{-3}$	$3.10 \times 10^{-3}$
PC: 0.8; PM: 0.01	52	$2.95 \times 10^{-3}$	$5.11 \times 10^{-3}$	$8.61 \times 10^{-3}$
PC: 0.5; PM: 0.01	51	$3.78 \times 10^{-3}$	$4.34 \times 10^{-3}$	$3.11 \times 10^{-2}$

### 3.4 Neural-ACO

The ACO parameters used in this research consist of pheromone constant ( $\alpha = 1$ ), heuristic constant ( $\beta = 1$  or  $\beta = 0$ ), pheromone evaporation rate ( $\rho = 0.1$  or  $\rho = 0.2$ ), number of ants = 50, number of iteration = 500 and best ants selected ( $k$  value = 8). Table 6 describes the performance of water content prediction using neural-ACO. The combination of  $\alpha = 1$ ,  $\beta = 1$  and  $\rho = 0.1$  had the lowest validation MSE ( $2.02 \times 10^{-3} \text{ (gg}^{-1}\text{)}^2$ ) on predicting water content of Sunagoke moss. Neural-ACO was also able to reduce irrelevant features and decrease the features from 106 to 10 features.

The pheromone evaporation rate  $\rho$  can be critical. The pheromone evaporation rate ( $\rho = 0.1$ ) had more accuracy on predicting water content based on validation MSE. Pheromone trail evaporation can be seen as an exploration mechanism that avoids quick convergence of all the ants towards a suboptimal path. An evaporation mechanism allows a continuous improvement of the learned problem structure. Evaporation decreases the pheromone trails with exponential speed.

Table 6. Performance of water content prediction using neural-ACO

ACO parameter	Number of Selected Features	Mean Square Error ( $\text{gg}^{-1}$ ) <sup>2</sup>		
		Training-set	Validation-set	Testing-set
$\alpha: 1; \beta: 1; \rho: 0.1$	10	$4.23 \times 10^{-3}$	$2.02 \times 10^{-3}$	$5.87 \times 10^{-3}$
$\alpha: 1; \beta: 1; \rho: 0.2$	21	$6.37 \times 10^{-3}$	$3.96 \times 10^{-3}$	$3.87 \times 10^{-3}$
$\alpha: 1; \beta: 0; \rho: 0.1$	13	$8.54 \times 10^{-3}$	$4.89 \times 10^{-3}$	$3.99 \times 10^{-3}$
$\alpha: 1; \beta: 0; \rho: 0.2$	7	$7.46 \times 10^{-3}$	$4.02 \times 10^{-3}$	$1.09 \times 10^{-2}$

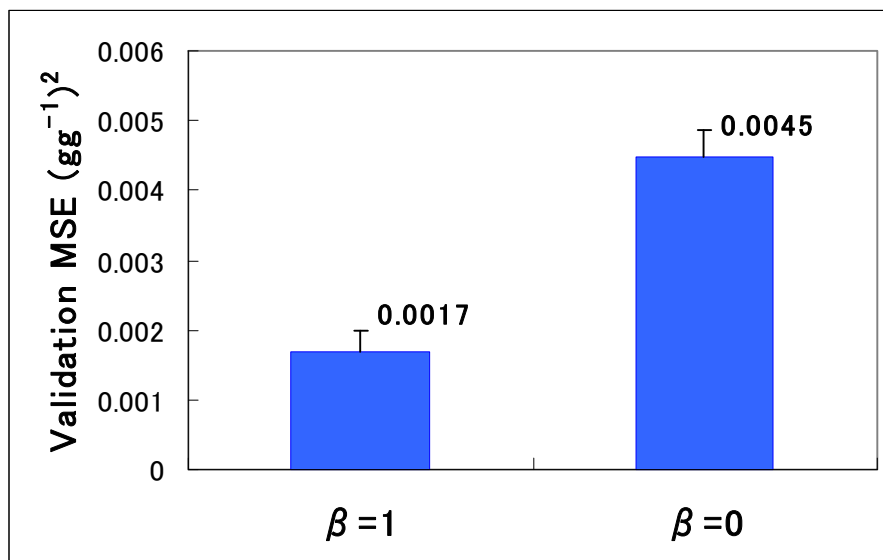
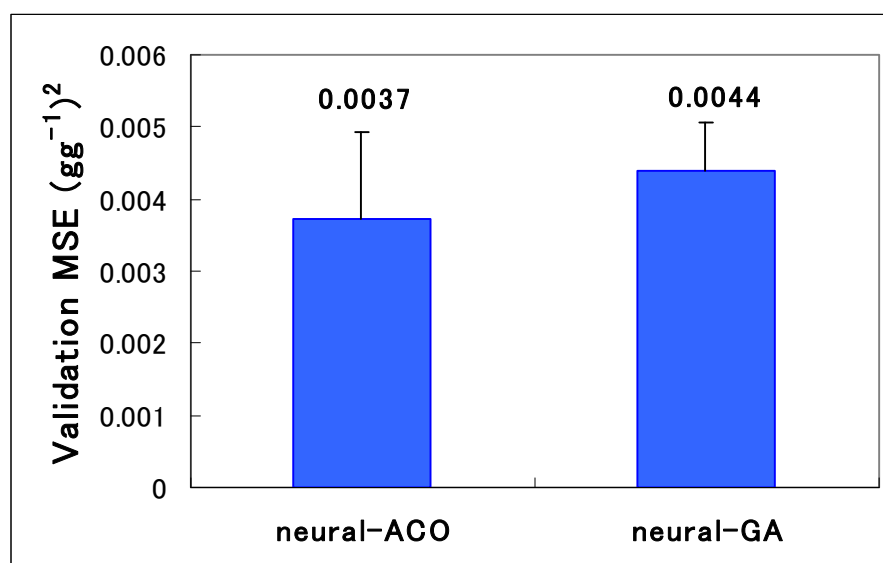


Figure 15. Comparison of  $\beta$  parameter in neural-ACO.

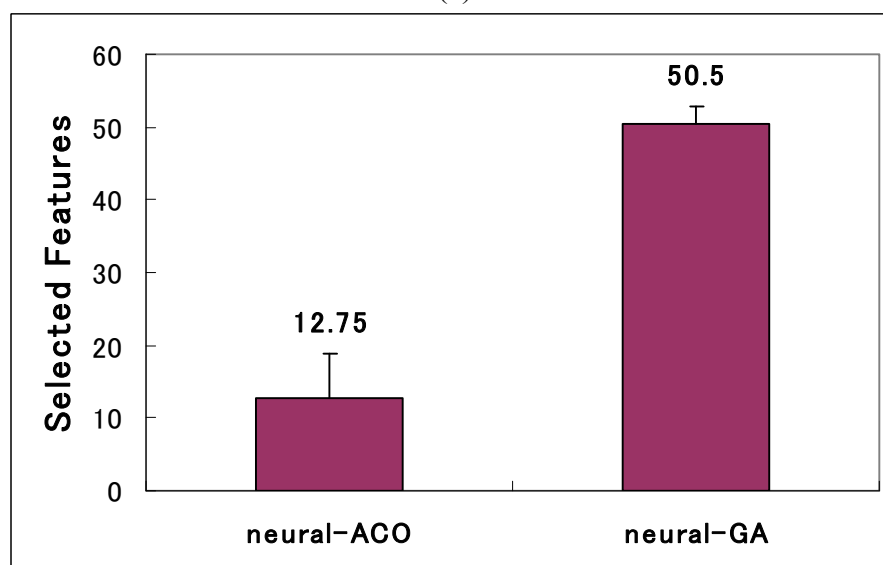
The possibility of using heuristic information to direct the ants' probabilistic solution construction is important because it gives the possibility of exploiting problem-specific knowledge. In this research we use *static* heuristic information where the values  $\eta$  are computed once at initialization time and then remain unchanged throughout the whole algorithm's run. Figure 15 shows that heuristic information  $\eta$  is important to be included. The value of  $\beta = 1$  means that heuristic information is considered to be as important as pheromone trails and the value of  $\beta = 0$  means that heuristic information is not included in the algorithm ( $\eta = 1$ ). Figure 15 shows that  $\beta = 1$  has better performance and better consistency for minimizing prediction error than  $\beta = 0$ . Furthermore, using analysis of *t-test* it was shown that there is a significant statistical improvement by using  $\beta = 1$  at  $\alpha = 0.01$  significant level.

The utilization of FS technique in selecting relevant features for predicting water content can be critical. Figure 16 shows the performance of two FS algorithms. It shows the superiority of neural-ACO for FS, since it achieved better prediction performance with lower number of features compare to neural-GA. From figure 16(a), we can see that neural-ACO (average validation MSE of neural-ACO =  $2.02 \times 10^{-3}$  ( $\text{gg}^{-1}$ )<sup>2</sup>) has lower average validation set MSE than neural-GA (average validation MSE of neural-GA =  $3.54 \times 10^{-3}$  ( $\text{gg}^{-1}$ )<sup>2</sup>), but there is no significant difference between their prediction performances. The results show that methods using FS (neural-GA and neural-ACO) has better result than methods without FS (MF, HSV CCM TF or HSL CCM TF). Furthermore, using analysis of *t-test* it was shown that there is a significant statistical difference between model using FS and model without FS at  $\alpha = 0.01$  significant level. The performance of BPNN model in both FS models (neural-GA and neural-ACO) for predicting water content of Sunagoke moss was satisfactory. The smallest training MSE of BPNN model less than 1% was obtained. From figure 16(b), neural-ACO has better performance for selecting relevant features than neural-GA and there is significant statistical difference between neural-ACO and neural-GA (*t-test* at  $\alpha = 0.01$  significant level). In conclusion, neural-ACO was tested successfully to find the best combination of relevant features and reduce the number of features in the feature-subset. The ten relevant features selected included: green canopy index MF, perimeter index MF, blue CCM energy TF, hue CCM contrast TF, hue CCM correlation TF, value<sub>(HSV)</sub> CCM correlation TF, hue CCM variance TF, hue CCM cluster tendency TF, green

CCM maximum probability TF and blue CCM maximum probability TF. ACO has powerful exploration ability. Several characteristics make ACO a unique approach: it is a constructive, population-based metaheuristic which exploits an indirect form of memory of previous performance. This combination of characteristics is not found in GA.



(a)



(b)

Figure 16. Comparison of neural-ACO and neural-GA based on: (a) validation MSE and (b) number of selected relevant image features.

#### 4. CONCLUSIONS

In conclusion, neural network model was able to correlate non-linear relationships between image features and water content. Morphological Features (MF), HSV Colour Co-occurrence Matrix Textural Features (HSL CCM TF) and HSL CCM TF were recommended as individual feature-subset to be used for predicting water content using Back-Propagation Neural Network

(BPNN) with average validation Mean Square Error (MSE) of  $6.70 \times 10^{-3} (\text{gg}^{-1})^2$ ,  $6.76 \times 10^{-3} (\text{gg}^{-1})^2$  and  $7.10 \times 10^{-3} (\text{gg}^{-1})^2$  in that order, respectively. However, the use of combination of some relevant image features for predicting water content shows better performance than individual feature-subset. Therefore, Feature Selection (FS) techniques have been proposed. The use of FS techniques has successfully selected relevant feature-subset to improve prediction performance. In this paper, we presented a novel FS search procedure for prediction based on Bio-inspired approaches. To show the utility of FS method we compare two proposed algorithms *i.e.* Neural-Genetic Algorithms (neural-GA) and Neural-Ant Colony Optimization (neural-ACO). The results show that neural-ACO has lower average validation set MSE than neural-GA, but there is no significant difference between their prediction performances. Neural-ACO has better performance for selecting relevant features than neural-GA and there is significant statistical difference between them (*t-test* at  $\alpha = 0.01$  significant level). Methods using FS has better result (average validation MSE of neural-GA =  $3.54 \times 10^{-3} (\text{gg}^{-1})^2$  and neural-ACO =  $2.02 \times 10^{-3} (\text{gg}^{-1})^2$ ) than methods without FS (MF, HSV CCM TF or HSL CCM TF). Furthermore, using analysis of *t-test* it was shown that there is a significant statistical difference between model using FS and model without FS at  $\alpha = 0.01$  significant level.

## 5. REFERENCES

- Ahmad, I. S., Reid, J. F. 1996. Evaluation of colour representations for maize images. *Journal of Agricultural Engineering Research* 63: 185-196.
- Angulo, J. and Serra, J. 2007. Modelling and segmentation of colour images in polar representations. *Image and Vision Computing* 25: 475-495.
- Bacci, L., Battista, P., Rapi, B. 2008. An integrated method for irrigation scheduling of potted plants. *Scientia Horticulturae* 116: 89-97.
- Cybenko, G. 1989. Approximation by superpositions of a sigmoidal function. *Mathematics of Control, Signals, and Systems* 2: 303-314.
- Dorigo, M. and Stutzle, T. 2004. *Ant Colony Optimization*. A Bradford book, The MIT Press, The United States of America.
- Escos, J., Alados, C. L., Pugnaire, F. I., Pigdefabregas, J., Emlen, J. 2000. Stress resistance strategy in an arid land shrub: interactions between developmental instability and fractal dimension. *Journal of Arid Environments* 45: 325-336.
- Foucher, P., Revollon, P., Vigouroux, B., Chasseriaux, G. 2004. Morphological image analysis for the detection of water stress in potted forsythia. *Biosystems Engineering* 89(2): 131-138.
- Goldberg, D.E. 1989. *Genetic algorithms in search, optimization and machine learning*. Kluwer Academic Publishers, Boston, MA.
- Graham, E. A., Hamilton, M. P., Mishler, B. D., Rundel, P. W., Hansen, M. H. 2006. Use of a network digital camera to estimate net CO<sub>2</sub> uptake of a desiccation-tolerant moss. *International Journal of Plant Sciences* 167(4): 751-758.
- Grande, F. D., Santomaso, A., Canu, P. 2008. Improving local composition measurements of binary mixtures by image analysis. *Powder Technology* 187(3): 205-213.
- Handels, H., Rob, T., Kreusch, J., Wolff, H. H., Poppl, S. J. 1999. Feature selection for optimized skin tumor recognition using genetic algorithms. *Artificial Intelligence in Medicine* 16: 283-297.
- Haralick, R. M., Shanmugam, K., Its'hak Dinstein. 1973. Textural features for image classification. *IEEE Transactions Systems Man and Cybernetics* 3(6): 610-621.

- Hendrawan, Y. and Murase, H. 2008. Intelligent irrigation control using colour, morphological and textural features in Sunagoke moss. An ASABE Annual International Meeting, Providence, USA, June 29-July 2, paper number: 083858.
- Hendrawan, Y. and Murase, H. 2009. Precision irrigation for Sunagoke moss production using intelligent image analysis. *Environmental Control in Biology* 47(1): 21-36.
- Holland, J. H. 1975. *Adaptation in natural and artificial systems*. University of Michigan Press, Ann Arbor.
- Igathinathane, C., Prakash, V. S. S., Padma, U., Ravi, B. G., Womac, A. R. 2006. Interactive computer software development for leaf area measurement. *Computers and Electronics in Agriculture* 51: 1-16.
- Kellner, E. 2001. Surface energy fluxes and control of evapotranspiration from Swedish sphagnum mire. *Agricultural and Forest Meteorology* 110: 101-123.
- Kurani, A. S., Xu, D. H., Furst, J. D., Raicu, D. S. 2004. Co-occurrence matrices for volumetric data. The 7th IASTED International Conference on Computer Graphics and Imaging - CGIM, Kauai, Hawaii, USA, in August 16-18.
- Kurata, K. and Yan, J. 1996. Water stress estimation of tomato canopy based on machine vision. *Acta Horticulturae* 440: 389-394.
- Leemans, V., Magein, H., Destain, M. F. 2002. On-line fruit grading according to their external quality using machine vision. *Biosystems Engineering* 83(4): 397-404.
- Murase, H., Honami, N., Nishiura, Y. 1994. Image information feedback using textural features for plant growth control. Proceedings of the First Asian Control Conference, Tokyo, 27-30 July, Vol.3, pp. 17-20.
- Murase, H., Nishiura, Y., Mitani, K. 1997. Environmental control strategies based on plant responses using intelligent machine vision technique. *Computers and Electronics in Agriculture* 18: 137-148.
- Newsam, S. and Kamath, C. 2005. Comparing shape and texture features for pattern recognition in simulation data. *IS&T/SPIE's Annual Symposium on Electronic Imaging*, San Jose, CA, United States January 16-20.
- Oechel, W. C. and Collins, N. J. 1976. Comparative CO<sub>2</sub> exchange in mosses from two tundra habitats at Barrow, Alaska. *Canadian Journal of Botany* 54(12): 1355-1369.
- Ondimu, S. N. and Murase, H. 2006. Thermal properties of living roof greening material by inverse modelling. *Applied Engineering in Agriculture* 22: 435-441.
- Ondimu, S. N. and Murase, H. 2008. Effect of probability-distance based Markovian texture extraction on discrimination in biological imaging. *Computers and Electronics in Agriculture* 63: 2-12.
- Patterson, D. W. 1996. *Artificial neural networks: theory and applications*. Prentice Hall, Singapore.
- Petrou, M. and Sevilla, P. G. 2006. *Image Processing: Dealing With Texture*. John Wiley and Sons, Chichester (2006).
- Recce, M., Taylor, J., Plebe, A., Tropiano, G. 1996. High speed vision-based quality grading of oranges. *International Workshop on Neural Networks for Identification, Control, Robotics and Signal/Image Processing*, pp 136-144. IEEE Computer Society Press, Venice, Italy.
- Saeyns, Y., Inza, I., Larranaga, P. 2007. A review of feature selection techniques in bioinformatics. *Bioinformatics* 23(19): 2507-2517.
- Utku, H. 2000. Application of the feature selection method to discriminate digitized wheat varieties. *Journal of Food Engineering* 46: 211-216.
- Verma, B. and Zhang, P. 2007. A novel neural-genetic algorithm to find the most significant combination of features in digital mammograms. *Applied Soft Computing* 7: 612-625.